Emergent Materials
https://doi.org/10.1007/s42247-024-00874-z

ORIGINAL ARTICLE

Sustained release investigation of curcumin and ciprofloxacin on coaxial electrospun nanocomposite scaffold of poly (3-hydroxybutyrate)-poly glycerol sebacate: an approach for skin regeneration

Seyed Mohammad Reza Hosseini[1] · Parisa Heydari[2] · Reyhaneh Nasr Azadani[2,3] · Siavash Iravani[4] · Ali Zarrabi[5,6,7]

Received: 10 July 2024 / Accepted: 15 September 2024

Abstract

The utilization of biomaterial scaffolds may promote the regeneration of cutaneous wounds. The investigation focused on fabricating an innovative type of scaffold for skin tissue regeneration through the coaxial electrospinning technique. The scaffold consisted of two segments: the core layer accommodated a combination of polyglycerol sebacate (PGS) and curcumin (Cur), while the shell layer contained poly(3-hydroxybutyrate) (PHB) and ciprofloxacin (CIP). An evaluation was conducted on the physical and mechanical properties, drug release characteristics, and cellular responses of the scaffolds. The assessment revealed that the fiber diameters and porosity of PGS/PHB and PGS/PHB-Cur/CIP were measured at 400–480 nm and 83–86%, respectively. The transmission electron microscopy (TEM) findings exhibited distinct core and shell structures in the PGS/PHB-Cur/CIP specimens. The specific aspects of the PGS/PHB-Cur/CIP scaffold, such as its controlled degradation (below 50% over 21 days), sustained drug release behavior of Cur and CIP (over 5 days), and optimal strength attributes (stress strength ~ 0.104 MPa), differentiate it from traditional wound coverings. Specifically, the incorporation of CIP and Cur into the fiber configuration enhanced the viability and adhesion of cells, resulting in an appropriate morphology. Therefore, the coaxial PGS/PHB-Cur/CIP demonstrates a heightened potential for wound dressing application or as a skin substitute.

Keywords Polyglycerol sebacate (PGS) · Curcumin (Cur) · Poly(3-hydroxybutyrate) (PHB) · Ciprofloxacin (CIP) · Coaxial electrospinning

✉ Parisa Heydari
parisa_heydari@alumni.iut.ac.ir

✉ Siavash Iravani
siavashira@gmail.com

✉ Ali Zarrabi
ali.zarrabi@istinye.edu.tr

[1] School of Medicine, Zanjan University of Medical Sciences, Zanjan, Iran

[2] Department of Biomaterials Nanotechnology and Tissue Engineering, School of Advanced Technology in Medicine, Isfahan University of Medical Sciences, Isfahan, Iran

[3] Biotechnology Department, Asu Vanda Gene Industrial Research Company, Tehran, Iran

[4] Independent Researcher, W Nazar ST, Boostan Ave, Isfahan, Iran

[5] Department of Biomedical Engineering, Faculty of Engineering and Natural Sciences, Istinye University, 34396 Istanbul, Türkiye

[6] Graduate School of Biotechnology and Bioengineering, Yuan Ze University, Taoyuan 320315, Taiwan

[7] Department of Research Analytics, Saveetha Institute of Medical and Technical Sciences, Saveetha Dental College and Hospitals, Saveetha University, Chennai 600 077, India

Published online: 03 October 2024

1 Introduction

The integumentary system consists of the skin, a type of connective tissue that acts as the body's largest organ and, in addition to maintaining physiological and biochemical conditions, shields it from external elements and harm [1, 2]. Notably, human skin functions as an intermediary between the body and its surroundings [3]. Various factors such as burns, traumas, diabetes, lacerations, and congenital irregularities, pose threats to the structural cohesion of the skin tissue, consequently impeding its physiological operations [4]. In addition, they lead to loss of body water, increased metabolism, and decreased body protein levels [5]. The wound healing process typically involves four primary stages: hemostasis (initiated immediately post-injury with platelet aggregation and blood clotting), inflammation (neutrophil migration to the wound site and release of inflammatory cytokines), tissue formation (granulation tissue formation at the wound site, fibroblast proliferation, and epithelialization), and tissue regeneration (collagen regeneration and scar tissue formation) [6–8]. If skin wounds are widespread, they lack the capacity for autonomous regeneration [9]. Thus, in order to mitigate inflammation and hemorrhaging, enhance cellular motility and proliferation, and ultimately enhance the process of wound healing, alternative methodologies must be employed [10]. One such approach involves the utilization of skin absorbable scaffolds fabricated through various techniques [11]. To ensure that these scaffolds serve not only as a conducive setting for cellular proliferation and attachment, but also as a means to establish an aseptic milieu through the eradication of excretions resulting from wounds and exudates, they are required to possess distinctive attributes including biocompatibility, antibacterial characteristics, biodegradation ratio, mechanical strength tailored to dermal specifications, and porosity conducive to cellular infiltration and nutrient diffusion [12–14].

Porous scaffolds are manufactured utilizing various methodologies such as phase separation, salt leaching, 3D printing, and electrospinning. Electrospinning, among the techniques mentioned, has been identified as a viable approach for the swift fabrication of micro/nano fibers according to electrohydrodynamic fundamentals [15, 16]. On the contrary, enhancements in the mechanical characteristics of electrospun nanofibers are achievable via the technique of coaxial electrospinning [17].Through this particular method, a broader spectrum of materials, natural or synthetic, can be utilized in fiber production, thanks to the variation in polymer compositions between the core and shell. Consequently, the establishment of a more robust electrospinning process is feasible, attributable to the generation of interface and adhesion phenomena [18]. Furthermore, the core-shell configurations offer the capability to encapsulate the medication into two components [19]. Due to the existence of the inner part, they have the potential to function as drug delivery systems for sustained release purposes [20]. Coaxial electrospinning provides significant advantages through facilitating the development of nanofibrous scaffolds using polymers and materials that are naturally unsuited for direct electrospinning. In addition, coaxial electrospinning eliminated the requirement for the same solvent for both polymers, hence reducing the likelihood of compatibility problems and changes in material characteristics caused by the solvent. This method allows the separate choice of solvents for each polymer, facilitating the modification of electrospinning conditions for both elements. Utilizing solvents that are specifically designed for each polymer guarantees the most efficient dissolving of the polymer and reduces the risk of unintended reactions or phase separation inside the electrospun fibers [19, 21, 22].

Poly-3 hydroxybutyrate (PHB), a member of the polyhydroxyalkanoates (PHAs) group, is a natural polymer derived from bacteria's sources such as *Ralstonia eutropha*, *Zoogloea ramigera*, *Escherichia coli*, and *Methylobacterium*, commonly utilized in tissue engineering, drug delivery, and medical applications [23, 24]. Biocompatibility, biodegradability, piezoelectric properties, high degree of crystallinity, and cell growth support are identified characteristics of PHB [25]. Its hydrophobic nature, low mechanical strength, and brittle structure limit its suitability for wound dressing application. Therefore, these limitations can be overcome by the incorporation of PHB with other polymers [26].

Poly(glycerol sebacate) (PGS) is a type of biodegradable polyester that is synthesized based on a polycondensation reaction involving sebacic acid and glycerol, demonstrating biocompatibility characteristics [27, 28]. The degree of synthesis significantly influences the chemical properties and degradation behavior of a material. In the synthesis of PGS, a flexible elastomer with nonlinear stress-strain behavior and shape memory, natural precursors such as glycerol and sebacic acid are utilized [29]. Owing to its limited specific surface area, the utilization of PGS within nanofiber configurations offers increased space for the migration of cells [30]. Selecting suitable biological materials and incorporating appropriate antibiotics can significantly enhance the efficacy of wound inflammation reduction and speed up wound healing. Although the PGS contain desirable physical and biological characteristics, it is limited in processing due to its low viscosity. This low viscosity prevents direct electrospinning, which is necessary for creating stable jets and continuous nanofibers that are essential for scaffold assembly. To address this difficulty and develop perfect control over the degradation kinetics, it is particularly beneficial

to combine polyesters and synthetic polymers that have different degradation profiles [31, 32].

In addition, the utilization of natural agents as medicine has received much attention due to their lesser side effects compared to chemical drugs, availability, and cost-effectiveness [33]. Curcumin (Cur), as a natural polyphenol derived from the rhizome of the turmeric plant, has been utilized in traditional Indian and Chinese remedy for numerous decades as an anti-inflammatory remedy for various ailments, such as liver disorders, rheumatoid arthritis, diabetes, and local ulcers [34, 35]. The antioxidant, antiseptic, anti-inflammatory, and favorable pharmacological characteristics of Cur have rendered it a potent and extensively employed substance in the domain of wound healing [36, 37]. Through the activation of cells to generate granulation tissue and assisting in collagen deposition, Cur exerts a crucial influence on the wound repair and the rejuvenation of impaired skin, thereby expediting the wound healing process [38].

Ciprofloxacin (CIP) is characterized as a hydrophobic antimicrobial agent possessing minimal toxicity and a substantial block concentration suitable for application in sustained drug delivery [39]. This drug has been selected as an appropriate antibiotic for wound healing due to its effect on a wide range of Gram-negative and positive bacteria and is encapsulated in electrospun membranes [40, 41].

In this investigation, nanocomposite scaffolds of PGS/PHB were developed using the core-shell electrospinning method, incorporating Cur and CIP drugs. In connection with this, following the PGS synthesis, the coaxial electrospinning of PGS/PHB with or without CIP and Cur was performed with the aim of fabrication of optimal scaffolds tailored for the regeneration of skin tissue. In addition, we conducted an examination of the chemical, mechanical, physical, and biological characteristics of polymers and medications to assess their suitability for utilization in wound dressings.

2 Materials and methods

2.1 Materials

PHB, sebacic acid monomer (99%), glycerol (99%), CIP, Cur, and glutaraldehyde were purchased from Sigma Aldrich (USA). Trifluoroacetic acid (TFA) and dimethyl sulfoxide (DMSO) were acquired from Merck (Germany). Phosphate-buffered saline, Dulbecco's Modified Eagle Medium-High Glucose (DMEM-High), penicillin/streptomycin, trypsin- ethylenediaminetetraacetic acid (EDTA), and methylthiazolyldiphenyltetrazolium bromide (MTT) kit were obtained from Bioidea (Iran). Fibroblast cell line (L929) was obtained from the Pasteur Institute (Iran).

2.2 Synthesis of PGS polymer

According to previous investigations, Sebacic acid (SA) and glycerol (Gly) were measured in equal molar amounts, following a 1:1 ratio by weight. The monomers were thorough vacuum drying at 60 °C for 24 h to remove any remaining moisture. The dehydrated monomers were moved to a three-necked round-bottom flask that was provided with a magnetic stirrer, a nitrogen input, and a condenser. To provide an environment free of reactivity, the flask was subjected to a 30 min purge of nitrogen gas. The flask was subsequently heated to a temperature of 120 °C while being continuously stirred, and it was kept at this temperature for a duration of 24 h. Throughout this period, the reaction mixture underwent continual purging with nitrogen gas to avoid oxidation and enhance the efficiency of polymerization. Following a period of 24 h, the combination undergoing the reaction was then cooled to a temperature range of 50 ± 5 °C. In the end, a PGS polymer with a white hue and a high level of viscosity was successfully produced [19].

2.3 Fabrication of coaxial electrospun scaffolds

The coaxial electrospun scaffolds construction involved dissolving PHB and PGS separately in trifluoroacetic acid (TFA) solvent at concentrations of 9% wt and 18% wt, respectively. Subsequently, CIP was incorporated into the shell (PHB solution) at a concentration of 3% w/v, followed by stirring for 10 min. Conversely, Cur was added to the PGS solution (considered as the core) at the concentration of 2% w/v and mixed for 20 min. Both solutions, shell and core, were electrospun at 0.2 mL/h flow rates and 1 mL/h, respectively, under a voltage of 27 ± 4 kV and a tip-to-collector distance of 17 cm, using a coaxial needle with specific dimensions. The core-shell samples were fabricated by electrospinning a solution of PGS or PGS/Cur and PHB or PHB/CIP onto a coaxial needle with an outer diameter (OD) and an inner diameter (ID) of 1 mm, and 0.4 mm, respectively.

2.4 Evaluation of coaxial wound dressing's morphology

The morphology of the PGS/PHB and PGS/PHB-Cur/CIP wound dressings was analyzed through scanning electron microscopy (SEM) utilizing a Philips XL30 system. The specimens were coated with gold prior to imaging, and images were taken at 12.0 kV under varying levels of magnification. Surface morphology analysis was conducted using ImageJ software (NIH&LOCI, USA) to ascertain

fiber diameter and distribution. A random selection of 25 fibers was analyzed to determine the average diameter and standard deviation. The pore size percentage of the scaffolds has been assessed using MATLAB (R2020a) software for the respective surfaces [21].

Transmission electron microscopy (TEM) images were employed to validate the presence of core-shell nanofibers and accurately measure their sizes. Fibers were electrospun onto a copper grid on the collector surface, and TEM images were captured using a Philips EM 208 S microscope from the Netherlands.

2.5 Chemical characterization

The examination of the chemical compositions of the PGS, PGS/PHB, and PGS/PHB-Cur/CIP sheets was conducted utilizing a Fourier transform infrared spectroscopy (FTIR) spectrometer (Bruker model; Karlsruhe company; Germany). The spectral analysis encompassed a range from 4000 to 400 cm^{-1}.

2.6 In vitro biodegradability assessment

Following the ASTM-F1635 standard, the dehydrated scaffolds were segmented into 1×1 cm^2 units and their initial weight were assessed. Subsequently, after immersing the scaffolds in 5 ml of phosphate-buffered saline (PBS) with a pH of 7.4, incubation was applied at 37 ± 3 °C for a duration of 21 days. At specific intervals (days 1,3,5,7,14,21), the scaffolds were extracted from the PBS solution, rinsed three times utilizing distilled water to effectively eliminate adsorbed pollutants, remove any remains from their surface and then subjected to a drying process in an oven for 5 h at a temperature of 37 ± 3 °C. After recalculating the weight, the weight loss percentage resulting from the biodegradation process was determined using Eq. 1.

$$Remaining\ weight\ (\%) = \frac{W_2 - W_1}{W_1} \times 100 \quad (1)$$

In this equation, W_2 denotes the weight of scaffolds upon degradation at particular times, while W_1 reveals the weight of the objects prior to being immersed in PBS [42].

After 21 days, SEM assessments had been done on the PGS/PHB and PGS/PHB-Cur/CIP specimens to evaluate the morphological changes observed during the degradation process.

2.7 Mechanical assay

A ZwickRoell electromechanical tensile tester (Germany) was used to measure the mechanical characteristics of the electrospun scaffolds. This approach adheres to the ASTM D882 standard, providing regularity and comparability with previous research. To this end, rectangular samples (3 cm x 1 cm) were precisely cut from the electrospun scaffolds. Then, the thickness of each sample was meticulously measured using a micrometer to ensure proper estimation of stress values. The specimens were firmly fixed in the grips of the tensile testing device, providing precise alignment and little movement during the experiment. The tensile test was performed at a consistent crosshead speed of 10 mm/min, a rate that biomaterials commonly use to replicate physiological loading conditions. The load cell, calibrated with a maximum value of 10 N, measured the force applied during the experiment, thus providing data on the scaffold's load-deformation characteristics. Specialized software examined the collected information, including the applied force and related elongation, to determine the scaffold's tensile strength, which is the highest level of stress that the scaffold may tolerate before it fails [43].

2.8 Drug delivery

To evaluate the delivery of CIP and Cur, we used a coaxial scaffold with or without drugs (2.5×2.5 cm^2). The scaffold was cultured in 10 ml of PBS (pH ~ 7.4), placed in a shaker incubator. The drug entrapment efficiency was then calculated over a period of 2 days at a temperature of 37 °C. Subsequently, the PGS/PHB-Cur/CIP sample and PGS/PHB (used as the control the specimen) were surrounded in a dialysis bag of a 10 kDa cut off. In the next step, after tightly sealing the bags, they were inserted into a flask filled with 100 mL of phosphate-buffered saline (PBS, pH 7.4). The flask was then subjected to continuous stirring at a speed of 100 revolutions per minute (rpm) at a temperature of 37 °C. A 100 µL sample of the medium that was removed was collected at specific times and examined using a UV-visible spectrophotometer at 360 nm and 272 nm to measure the concentrations of Cur and CIP, respectively. Subsequently, a refresh PBS was launched at consistent time intervals. Using the calibration curve, the quantities of Cur and CIP that were released at each specified time period were determined.

2.9 Cell viability and morphology

The L929 murine fibroblast cell line was cultured in DMEMF High Glucose Media supplemented with 10% v/v FBS and 1% v/v streptomycin/penicillin. The preserving of cells was performed under controlled conditions at a steady temperature of 37 °C and a humidified environment that contains 5% CO_2. For cell passaging, the cells in the culture

plate were rinsed with PBS and eventually treated using a 0.25% Trypsin/EDTA solution for 2 min.

Using a skin punch with a diameter of 7 mm, circular samples were prepared from PGS/PHB and PGS/PHB-Cur/CIP scaffolds. They were then sterilized in three steps: first, by washing with PBS, followed by ethanol treatment, and lastly exposed to UV radiation for was carried out to prevent contamination before the scaffolds on 48-well plates for cell culture. Therefore, a total of 10^4 cells were placed in each well of the samples and tissue culture plate (TCP) as the control. Subsequently, the cell-containing samples were subjected to a 7-day incubation period, during which the culture medium was refreshed every 2 days.

The MTT assay was applied to determine the relative cell viability. The growth medium was taken away on days 1, 3, and 7, and 100 µL of MTT solution (5 mg/mL) was added to the samples with cells and the control. The samples were then incubated for 4 h. Upon dissolution of the dark blue formazan crystals in DMSO, 100 µL were subsequently dispensed from each sample into a 96-well plate. The optical density (OD) of the solution was then determined at 490 nm via an ELISA reader (Biorad-USA). Equation 2 was implemented to ascertain the percentage of relative cell survival:

$$Relative\ cell\ survival\ (\%control) = \frac{OD_{Sample} - OD_{Blank}}{OD_{Control} - OD_{Blank}} \times 100 \quad (2)$$

Where OD_{sample} was the optical densities of PGS/PHB and PGS/PHB-Cur/ CIP samples, and the OD_{blank} and $OD_{control}$ were the optical densities of DMSO (blank) and TCP (control), respectively [44].

To examine the adherence and spreading of L929 cells on the membranes, the specimens were washed with PBS solution and then treated with 1.5% glutaraldehyde for 4 h at a temperature of 4 °C, three days after the cells were seeded. Following the PBS wash, the samples were subsequently immersed in alcohol solutions with increasing concentrations, ranging from 50 to 100%, to facilitate dehydration. The specimens were observed utilizing SEM (Philips); however, prior to this procedure, a layer of gold was deposited onto the specimens.

2.10 Statistical analysis

The data was analyzed by statistical analysis using the ANOVA test. The Tukey-Kramer post hoc test was utilized with GraphPad Prism Software (Version 9) to identify the significant difference between groups. A p-value below 0.05 was utilized illustrate statistical significance.

3 Results and discussion

3.1 Morphological assessment

3.1.1 SEM

The PGS/PHB electrospun skin dressing had a thickness of 442 ± 30 µm, indicating a strong and durable structure. After addition of CIP and Cur, a decrease in thickness to 327 ± 30 µm was observed. The reduction in thickness implies a possible alteration in the structure or compactness of the scaffold, which may impact its mechanical properties and physical and biological activity [45].

Relevant parameters such as the distribution of fiber diameter, the percentage of porosity, and the uniformity determine the cell behavior in electrospun wound dressing. Figure 1 A displays SEM images of PGS/PHB and PGS/PHB-Cur/CIP scaffolds, with two scale bars measuring 50 µm and 10 µm, respectively. The SEM images provide conclusive proof that, when using the specified electrospinning settings, the process successfully produces uniform fibers without any bead developments. Nevertheless, the inclusion of drugs resulted in a decrease in the diameter of the fiber. The average diameter of the PGS/PHB sample was 486.6 ± 20 nm but the diameter of the fibers in samples containing Cur and CIP was measured to be 400.2 ± 14 nm. This shows that the difference is statistically significant ($p < 0.05$) when compared to the fibers in samples without drugs, using the PGS/PHB scaffold. Numerous investigations demonstrated a decrease in viscosity of polymeric solutions when drugs such CIP and Cur are added. Some drugs have the ability to disrupt the intermolecular connections inside polymers and position themselves along the polymer chains [46, 47]. Consequently, the chemical connection between polymer chains would be interrupted. These occurrences may lead to a decrease in viscosity and have an impact on the diameter of the fibers [48]. Porosity is an essential feature, along with fiber diameter, to assess the structure of skin tissue engineering scaffolds. Interconnected porous scaffolds enhance nutrient delivery to deeper layers, enabling cell viability in these areas [49, 50]. In this work investigated the porosity of the PGS/PHB and PGS/PHB-Cur/CIP scaffolds by utilizing SEM images and MATLAB software. The porosity percentages of PGS/PHB and PGS/PHB-Cur/CIP were determined to be $83.2 \pm 4\%$ and $86.1 \pm 3\%$, respectively. The results showed that the PGS/PHB based wound dressing had a porosity of above 80%, and there was no significant difference between the dressings with or without Cur/CIP drugs. Moreover, the interconnectedness of pores creates hydrodynamic microenvironments through which diffusion proceeds. A surface that has the right amount of porosity also creates a mechanical connection between the scaffold and

the surrounding tissue during the process of regeneration. This connection improves the entire mechanical stability at the border. Based on the literature, a minimum necessary value of 80% porosity is reported for the development of a 3D matrix that allows cell penetration in scaffolds [51]. Hence, the incorporation of Cur/CIP into PGS/PHB fibers leads to a reduction in the fibers' diameter while still offering adequately porous structure for tissue engineering applications.

3.1.2 TEM

One of the most appropriate assays to evaluate the internal structure of nanofibers and nanoparticles is the use of TEM images. Figure 1B presents the TEM pictures of PGS-PHB-Cur/CIP core-shell specimens following the morphological evaluation of fiber. PGS-Cur exists within the internal dark regions of the nanofiber. The TEM images reveal the formation of a coaxial structure within a nanofiber, where the core layer a darker appearance compared to the shell layer. As illustrated in Fig. 1B, the PGS/PHB-Cur/CIP wound dressing encompasses a core region that represents roughly 30% of the total diameter of the fibers. Within the PGS/PHB-Cur/CIP membrane, the diameter of the fibers was recorded at 405.2 ± 23 nm, whereas the core area had a diameter of 130.5 ± 20 nm. The distinction in electron beam transmissibility between the PGS and PHB regions gives rise to the contrast observed between the core and shell layers of the fiber [19]. In this study, results demonstrated the different occurrences within the core, indicating that the core's volume was smaller than what could be elongated by the shell's viscous drag forces. Enhancing the size of the core fiber in comparison to the shell one, enhances its physical, mechanical, and drug release behavior [21].

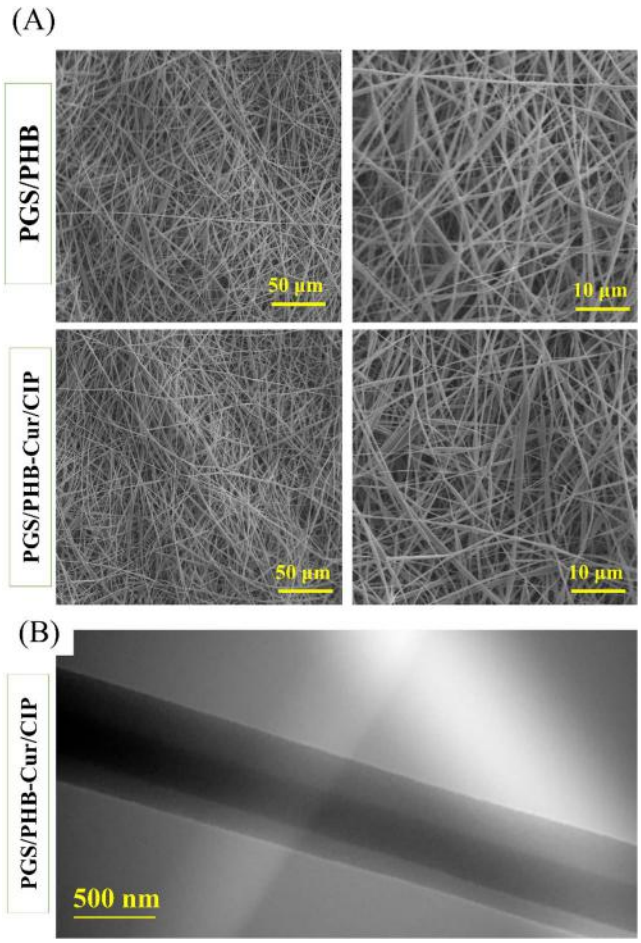

Fig. 1 **A** SEM images of coaxial PGS/PHB and PGS/PHB-Cur/CIP fibers with various scale bar such as *10 µm* and *50 µm* and **B** TEM image of PGS/PHB-Cur/CIP coaxial wound dressing fiber (*scale bar: 500 nm*)

3.2 Chemical characterization

The study developed a coaxial PGS/PHB composite with or without Cur/CIP membrane to accelerate the procedure of wound healing. The FTIR spectra of coaxial PGS/PHB, and PGS/PHB-Cur/CIP scaffolds, in the range of 400–4000 cm^{-1}, has been depicted in Fig. 2. The peaks seen in the FTIR spectrum at around 1044 cm^{-1} (C-CH_3 stretching), 1054 cm^{-1} (C-O), 1130 cm^{-1} (CH_3 rocking), 1224 cm^{-1} (C-O-C stretching), 1287 cm^{-1} (CH), 1380 cm^{-1} (CH_3), and 1450 cm^{-1} (C = O stretching) can be attributed to the PHB polymer. Hence, the peaks seen at 1159 cm^{-1} and 3448 cm^{-1} can be attributed to the C-O and O-H functional groups present in the PGS polymers [19]. The presence of the PGS and PHB in the structure of core-shell electrospun scaffold was confirmed by the presence of these specific peaks. Subsequently, the FTIR spectra of PGS/PHB-Cur/CIP exhibited a broad band, which proved the presence of Cur/CIP in the designed wound dressing. The peak seen at 1277 cm^{-1} corresponds to the bending vibration of the C-O phenolic band of Cur. On the other hand, the peak observed at 1624 cm^{-1} is associated with CIP [19, 22].

3.3 Degradation behavior

The degradation properties of a scaffold are crucial and indispensable factors to consider when evaluating wound dressing agents. The physicochemical characteristics and porous structure of the scaffold have a substantial impact on its degradation performance [52]. There is an accepted theory that non-degradable biomaterials within the human organism can result in a prolonged inflammatory response over time, which could be due to a failure in the implantation process [53]. An optimal biomaterial scaffold for tissue regeneration should possess a uniform degradation rate when combined with the regeneration of new tissue [54]. Nevertheless, the process during which PGS/PHB and PGS/

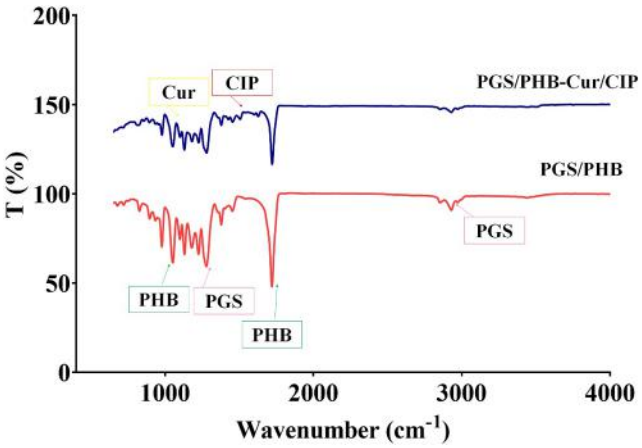

Fig. 2 FTIR of PGS/PHB and PGS/PHB-Cur/CIP scaffolds in the region of 1100–1700 cm^{-1}

PHB-Cur/CIP degrade in a biological environment remains very intricate due to the presence of several active components inside cells and extracellular fluid, as well as the complex structure of the polymer. When studying the healing of skin wounds, the usual method to assess the durability of a scaffold is by conducting an in vitro degradation test. This involves measuring the change in weight of the samples immersed in PBS at 37 °C, under certain pH conditions that simulate the physiological environment [52]. Figure 3 A displays the degradation characteristics of the PGS/PHB and PGS/PHB-Cur/CIP in PBS at 37 ◦C during a 21-day period. The coaxial electrospun scaffold exhibited a consistent and regulated degradation rate during the whole 21-day incubation period. Our investigation revealed a degradation profile consisting of three distinct stages: the first stage, which covers the first day; the second stage, which includes days 1 to 3; and the third stage, which extends from day 3 to 21. During the 1st and 2nd stages, the rate of weight loss was slowed. This slight degradation can be attributed to the chemical reaction of the polymer's backbone [55]. This degradation created an opportunity for the release of drugs and the penetration of water molecules into the chemical structure [56]. After 7 days of incubation, the PGS/PHB and PGS/PHB-Cur/CIP scaffolds weight loss of $90.04 \pm 4\%$ and $81.23 \pm 2\%$, respectively. It can be said at the last degradation stage, the PGS/PHB-Cur/CIP saw significant weight loss due to the breakdown of polymers, Surface degradation of PGS and rapid degradation under simulated physiological conditions. This stage resulted from the severe physical and chemical breakdown of the polymer network, in addition to an inadequate amount of remaining unreacted components. In addition, it was demonstrated that the inclusion of drugs such as Cur and CIP resulted in an increased degradation rate of the samples as the fastest degradation was seen in the case of PGS/PHB-Cur/CIP. The result was entirely consistent with the findings of the prior investigation [19, 22]. These wound dressings, based on PGS/PHB, have the required biodegradable characteristics to be absorbed by nearby tissue and generate their own extracellular matrix (ECM) [57].

The impact of a 21-day immersion in PBS on the scaffolds was analyzed using SEM analysis (Fig. 3B). The morphology of all the electrospun fibers exhibited fractures in the scaffolds, however, a greater quantity of break-in fibers were observed in the PGS/PHB-Cur/CIP membranes in comparison to the PGS/PHB samples.

3.4 Mechanical assay

Optimum wound dressings require both strength and flexibility, which are mechanical critical qualities. A wound dressing must possess enough resilience to provide protection against external pressures, while also maintaining sufficient flexibility to prevent damage to the underlying tissues during movement [58]. Furthermore, possessing desirable mechanical characteristic is requisite for facilitating the growth and specialization of cells. It should be noted that the mechanical features of electrospun samples are influenced by the average fiber diameter, chemical composition, fiber form, and their homogeneity [59, 60]. The current work investigated tensile strength, the stress-strain characteristics, and elongation of scaffolds constructed with PGS/PHB and PGS/PHB-Cur/CIP (Fig. 4A-C). The results indicated that the PGS/PHB scaffolds exhibited the highest stress strength value in comparison with PGS/PHB-Cur/CIP. The stress strengths of PGS/PHB and PGS/PHB-Cur/CIP scaffolds were determined to be 0.133 ± 0.04 MPa and 0.104 ± 0.07 MPa, respectively. This study revealed that by adding drugs into fiber and the reduction of fiber diameters resulted in a decrease in tensile strength. Figure 4B and SEM analysis revealed that incorporating Cur and CIP into the core and shell of fibers led to alterations in fiber shape and diameter. These modifications are crucial in defining the mechanical characteristics of electrospun scaffolds. Previous research has shown that reducing the diameter of fibers leads to a decrease in their tensile capacity [21]. Kim et al. [61] observed that PCL mats with higher average fiber diameters exhibited greater strength. They also established a substantial correlation between the mechanical characteristics of electrospun membranes and their fiber shape, including average fiber size. Based on the current investigation, the addition of Cur and CIP to the core and shell of fiber resulted in a decrease in diameter, as well as a considerable reduction in strength.

According to the tensile assay results, adding drugs to the structure did not result in significant differences in elongation. Similarly, Dorri et al. [13] showed that the optimal stress strength for wound dressing is about 0.09 MPa.

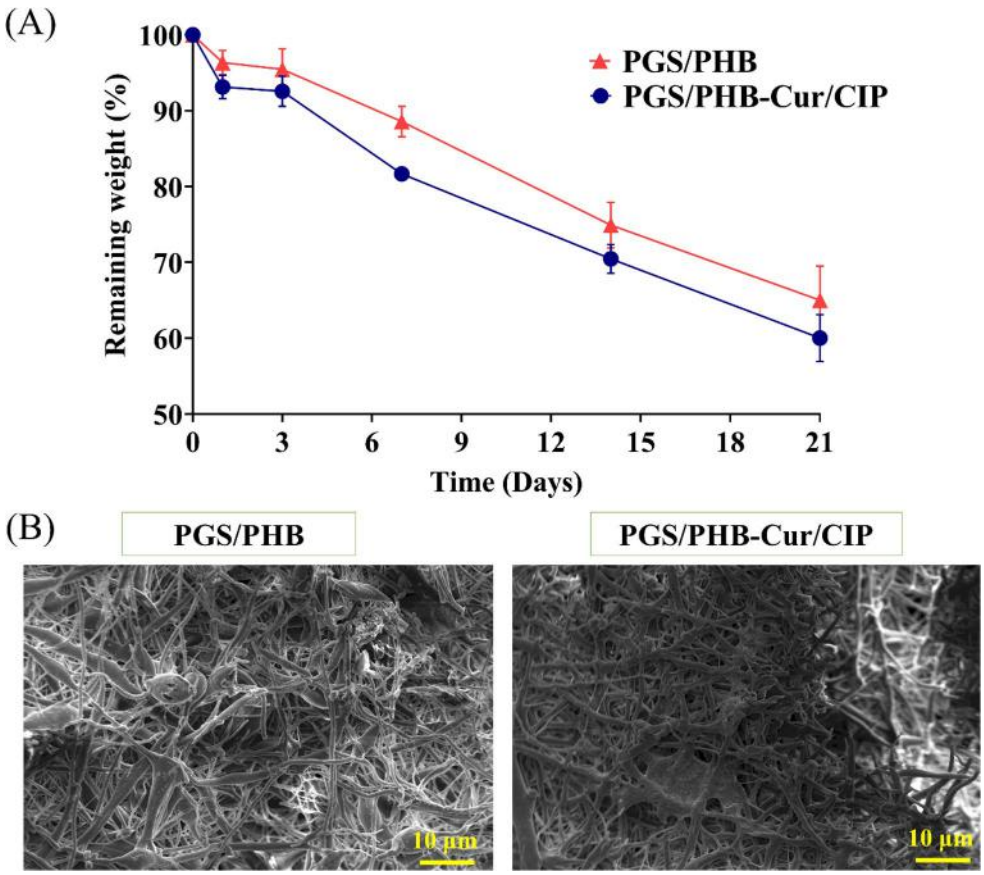

Fig. 3 **A** weight loss (%) of PGS/PHB and PGS/PHB-Cur/CIP scaffolds during 21 days of degradation in PBS pH ~ 7.4 and 37 °C temperature and **B** SEM images of coaxial PGS/PHB and PGS/PHB-Cur/CIP fibers after 21 days degradation with various *scale bar* such as *10 µm* and *50 µm*. All values are defined as being representative of the means ($n = 3$) ± standard deviation

Considering their mechanical and physical properties, PGS/PHB and PGS/PHB-Cur/CIP composites appear to be suitable candidates for skin tissue engineering applications.

3.5 Drug delivery

The nanofibers containing Cur and CIP had drug loading efficiencies of 95% (680 ± 12 µg) and 92% (51.3 ± 6 µg) respectively, indicating the remarkable efficiency of core-shell fibers in encapsulating drug molecules (1 × 1 cm^2 of wound dressing).

The release patterns of PGS/PHB-Cur/CIP were shown in Fig. 5A, exhibiting the Cur and CIP release rates. Nanofibers fabricated of hydrophobic PHB and Cur were able to release Cur continuously without a burst release at the beginning. The rate at which CIP was released was quicker than Cur, mostly because to the enhanced hydrophilic properties of CIP within the fiber shell. The rapid release of CIP can be attributed to the significant shell-to-core volume ratio of the fibers, as seen in Fig. 1B. According to the continuous release Cur profile from the PGS/PHB scaffold profile, it can be said that it is Due to the hydrophobic nature of the polymer PHB, the shell layer of nanofibers exhibited hydrophobic properties. This hydrophobic surface prevented the medium from easily penetrating into the core layer, leading to a prolonged release of Cur at a physiological pH of ~ 7.4 [62]. While the rapid release of CIP can be attributed to the significant shell-to-core volume ratio of the fibers, this problem results in a greater probability of the contact surface having water molecules and the quick CIP release [63].

Previous studies indicated that the initial release of the antibacterial drug effectively inhibited bacterial growth. Additionally, the sustained release of the anti-inflammatory and antioxidant drugs accelerates the wound healing process and improves overall wound healing [22, 42].

3.6 Skin cell behavior

The L929 cell line is widely used for wound healing applications [64]. The present study evaluated the biocompatibility of PGS/PHB, PGS/PHB-Cur, PGS/PHB-CIP, and PGS/PHB-Cur/CIP using the L929 cell line (Fig. 5B). In order to examine the biocompatibility of the items, L929 cells were cultured over the scaffolds. According to the data shown in Fig. 5B, PGS/PHB, PGS/PHB-Cur, PGS/PHB-CIP, and PGS/PHB-Cur/CIP had comparable cell viability. The cell viability of these samples was much greater than that of a tissue culture plate (TCP, negative control). Following a 7-day incubation period, the cell survival rates exhibited a considerable rise in all wound dressings. This indicates that

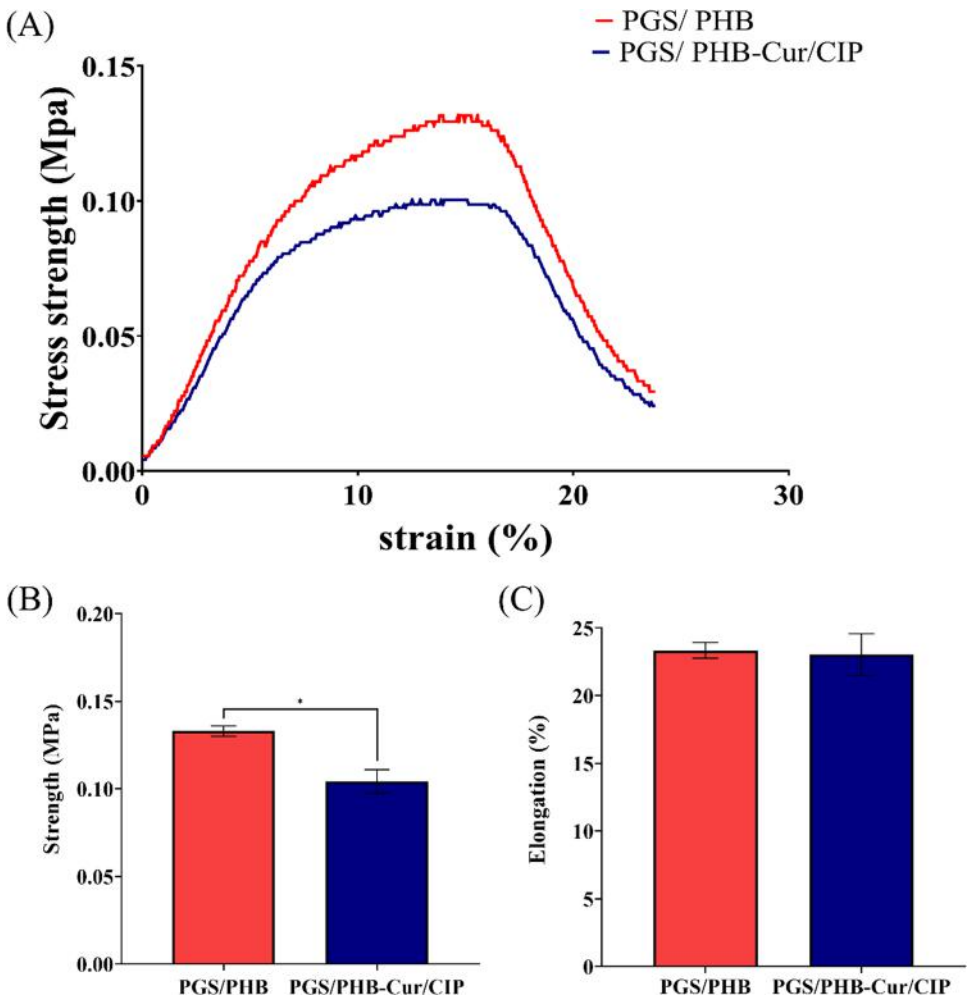

Fig. 4 Mechanical characteristics of PGS/PHB and PGS/PHB-Cur/CIP: **A** Stress-strain curves, **B** tensile strength, and **C** elongation of samples. Each of the values are classified as being representative of the means ($n=3$) ± standard deviation. (*: $P<0.05$)

our developed PGS/PHB, PGS/PHB-Cur, PGS/PHB-CIP, and PGS/PHB-Cur/CIP samples do not possess any adverse effects.

The findings also indicated that the rates of cell growth and cell adhesion in PGS/PHB-Cur/CIP were notably greater than those observed in PGS/PHB samples (Fig. 5C).

The cellular response demonstrated that PGS/PHB, with or without Cur/CIP, exhibited excellent cell viability and cell growth within the L929 cell line. Following a 7-day incubation period, the cell survival rates exhibited a considerable rise in all wound dressings. This indicates that our developed PGS/PHB and PGS/PHB-Cur/CIP samples do not possess any adverse effects.

Remarkably, the combination of drugs with PGS/PHB demonstrated comparable or even superior cell biocompatibility when compared to PGS/PHB wound dressing. This might be because of the sustained release of Cur, which improved skin cell growth. Similarly, Vater et al. [65] set up an evaluation of nanoemulsions containing lecithin, both with and without Cur. They demonstrated that the release of Cur resulted in an improvement in the proliferation and cell survival of human keratinocytes and fibroblast cells for wound healing applications.

Based on these results, we can say that the PGS/PHB-Cur/CIP coaxial electrospun scaffold can help cells grow and would be good for more experiments that take place in living things. In future studies, it is necessary to assess the safety of wound dressings and their by-products when they dissolve and degrade during in vivo characterization. The next step is to develop a suitable animal model to assess the safety and efficacy of PGS/PHB-Cur/CIP for use as a wound dressing or skin substitute.

4 Conclusion

The present investigation successfully developed a novel coaxial PGS/PHB-Cur/CIP electrospun scaffold, demonstrating its potential in accelerating wound healing application. The developed wound dressing had the uniform structure based on nanofibers, controlled degradation rate, and desirable mechanical properties, as well as the

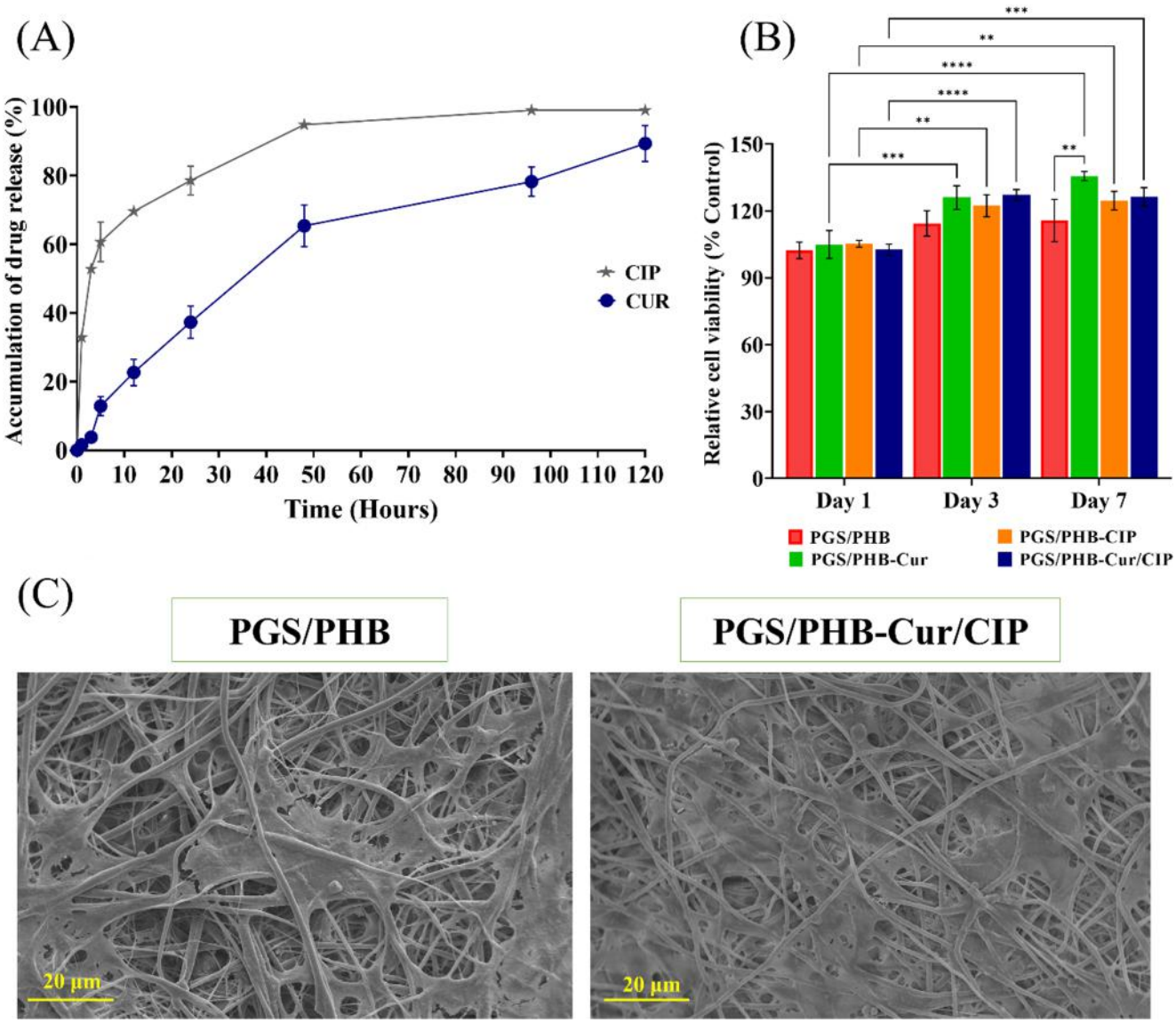

Fig. 5 **A** In vitro CIP and Cur cumulative release of PGS/PHB samples incubated in PBS for 5 days at pH 7.4, **B** The relative L929 cell viability when in contact with PGS/PHB, PGS/PHB-Cur, PGS/PHB-CIP, and PGS/PHB-Cur/CIP scaffold, evaluated using the MTT assay over 7 days. The obtained results were normalized against the control group (TCP), and **C** SEM image of L929 cultured on PGS/PHB and PGS/PHB-Cur/CIP scaffolds at days 3 (*scale bar: 20 µm*). The statistics are displayed as the means ($n=3$) ± standard deviation. (**: $p<0.01$ and ***: $p<0.001$)

ability to release both Cur and CIP in a controlled way. The biocompatibility of the PGS/PHB-Cur/CIP scaffold was demonstrated through in vitro studies, which remarkable cell proliferation and adhesion abilities in L929 fibroblasts. The simultaneous inclusion of antibacterial and anti-inflammatory drugs in the scaffold shows great potential in creating an optimal environment for wound healing.

Future study should concentrate on the treatment of wounds in animal models, assessment of immunomodulation responses, and investigation of the practicality and safety of using this technology in a clinical environment, using preclinical studies. This innovative approach of wound care has immense potential for enhancing patient results and might have a substantial influence on the field of regenerative medicine.

Declarations

Competing interest The author(s) declare no competing interest.

References

1. M. Venus, J. Waterman, I. McNab, Basic physiology of the skin. Surg. **28**(10), 469–472 (2010)

2. A. Keirouz, M. Chung, J. Kwon, G. Fortunato, N. Radacsi, 2D and 3D electrospinning technologies for the fabrication of nanofibrous scaffolds for skin tissue engineering: a review. Wiley Interdiscip Rev. Nanomed. Nanobiotechnol. **12**(4), e1626 (2020)
3. A. Fakouri, Z.-S. Razavi, A.T. Mohammed, A.H.A. Hussein, H. Afkhami, M.H. Hooshiar, Applications of mesenchymal stem cell-exosome components in wound infection healing: new insights. Burn Trauma. **12**, tkae021 (2024)
4. B. Veleirinho, D.S. Coelho, P.F. Dias, M. Maraschin, R.M. Ribeiro-do-Valle, Lopes-da-Silva, Nanofibrous poly (3-hydroxybutyrate-co-3-hydroxyvalerate)/chitosan scaffolds for skin regeneration. Int. J. Biol. Macromol. **51**(4), 343–350 (2012)
5. C. Wei et al., Biomaterials in skin tissue engineering. Int. J. Polym. Mater. Polym. Biomater. **71**(13), 993–1011 (2022)
6. D. Akbik, M. Ghadiri, W. Chrzanowski, R. Rohanizadeh, Curcumin as a wound healing agent. Life Sci. **116**(1), 1–7 (2014)
7. G. Topman, F.-H. Lin, A. Gefen, The natural medications for wound healing–curcumin, aloe-vera and ginger–do not induce a significant effect on the migration kinematics of cultured fibroblasts. J. Biomech. **46**(1), 170–174 (2013)
8. Y. Yen et al., Curcumin accelerates cutaneous wound healing via multiple biological actions: the involvement of TNF-α, MMP-9, α-SMA, and collagen. Int. Wound J. **15**(4), 605–617 (2018)
9. M. Rostami et al., The role of Dental-derived stem cell-based therapy and their derived extracellular vesicles in post-COVID-19 syndrome-induced tissue damage. Stem Cell. Rev. Rep. **1**, 1–42 (2024)
10. M. Hosseini Hooshiar et al., The potential use of nanozymes as an antibacterial agents in oral infection, periodontitis, and periimplantitis. J. Nanobiotechnol. **22**(1), 207 (2024)
11. Y. Liu, Y. Zheng, B. Hayes, Degradable, absorbable or resorbable—what is the best grammatical modifier for an implant that is eventually absorbed by the body? Sci. China Mater. **5**(60), 377–391 (2017)
12. A.A. Chaudhari et al., Future prospects for scaffolding methods and biomaterials in skin tissue engineering: a review. Int. J. Mol. Sci. **17**(12), 1974 (2016)
13. Y.D. Nokoorani, A. Shamloo, M. Bahadoran, H. Moravvej, Fabrication and characterization of scaffolds containing different amounts of allantoin for skin tissue engineering. Sci. Rep. **11**(1), 16164 (2021)
14. T. Agarwal et al., Gelatin/Carboxymethyl chitosan based scaffolds for dermal tissue engineering applications. Int. J. Biol. Macromol. (2016). https://doi.org/10.1016/j.ijbiomac.2016.04.028
15. R. Augustine et al., Cerium oxide nanoparticle incorporated electrospun poly (3-hydroxybutyrate-co-3-hydroxyvalerate) membranes for diabetic wound healing applications. ACS Biomater. Sci. Eng. **6**(1), 58–70 (2019)
16. N.H. Kouchehbaghi et al., A machine learning-guided design and manufacturing of wearable nanofibrous acoustic energy harvesters. Nano Res. **17**, 1–12 (2024)
17. Q. Hu, C. Wu, H. Zhang, Preparation and optimization of a biomimetic triple-layered vascular scaffold based on coaxial electrospinning. Appl. Biochem. Biotechnol. **190**(3), 1106–1123 (2020)
18. G.-Z. Yang, J.-J. Li, D.-G. Yu, M.-F. He, J.-H. Yang, G.R. Williams, Nanosized sustained-release drug depots fabricated using modified tri-axial electrospinning. Acta Biomater. **53**, 233–241 (2017)
19. P. Heydari, J. Varshosaz, A. Zargar Kharazi, S. Karbasi, Preparation and evaluation of poly glycerol sebacate/poly hydroxy butyrate core-shell electrospun nanofibers with sequentially release of ciprofloxacin and simvastatin in wound dressings. Polym. Adv. Technol. **29**(6), 1795–1803 (2018)
20. B. Xu et al., Non-linear elasticity of core/shell spun PGS/PLLA fibres and their effect on cell proliferation. Biomaterials. **34**(27), 6306–6317 (2013)
21. S. Shafizadeh, P. Heydari, A. Zargar Kharazi, L. Shariati, Coaxial electrospun PGS/PCL and PGS/PGS-PCL nanofibrous membrane containing platelet-rich plasma for skin tissue engineering. J. Biomater. Sci. Polym. Ed. **35**, 1–19 (2023)
22. P. Heydari, A. Zargar Kharazi, S. Asgary, S. Parham, Comparing the wound healing effect of a controlled release wound dressing containing curcumin/ciprofloxacin and simvastatin/ciprofloxacin in a rat model: a preclinical study. J. Biomed. Mater. Res. Part. A. **10**, 341–352 (2021)
23. H.S. Kim et al., Prevention of excessive scar formation using nanofibrous meshes made of biodegradable elastomer poly (3-hydroxybutyrate-co-3-hydroxyvalerate). J. Tissue Eng. **11**, 2041731420949332 (2020)
24. S. García-Cerna et al., Evaluation of Poly-3-Hydroxybutyrate (P3HB) scaffolds used for epidermal cells growth as potential biomatrix. Polym. (Basel). **14**(19), 4021 (2022)
25. A.S. Arampatzis et al., Novel electrospun poly-hydroxybutyrate scaffolds as carriers for the wound healing agents alkannins and shikonins. Regen Biomater. **8**(3), rbab011 (2021)
26. F. Erci, F.B. Sariipek, Fabrication of antimicrobial poly (3-hydroxybuthyrate)/poly (ε-caprolactone) nanofibrous mats loaded with curcumin/β-cylodextrin inclusion complex as potential wound dressing. J. Drug Deliv Sci. Technol. **89**, 105023 (2023)
27. L. Vogt, F. Ruther, S. Salehi, A.R. Boccaccini, Poly (glycerol sebacate) in biomedical applications—a review of the recent literature. Adv. Healthc. Mater. **10**(9), 2002026 (2021)
28. M. Rostamian, M.R. Kalaee, S.R. Dehkordi, M. Panahi-Sarmad, M. Tirgar, V. Goodarzi, Design and characterization of poly (glycerol-sebacate)-co-poly (caprolactone)(PGS-co-PCL) and its nanocomposites as novel biomaterials: the promising candidate for soft tissue engineering. Eur. Polym. J. **138**, 109985 (2020)
29. G. Matyszczak, M. Wrzecionek, A. Gadomska-Gajadhur, P. Ruśkowski, Kinetics of polycondensation of sebacic acid with glycerol. Org. Process. Res. Dev. **24**(6), 1104–1111 (2020)
30. X. Yang, L. Li, D. Yang, J. Nie, G. Ma, Electrospun core–shell fibrous 2D scaffold with biocompatible poly (glycerol sebacate) and poly-l-lactic acid for wound healing. Adv. Fiber Mater. **2**(2), 105–117 (2020)
31. P. Khaloo Kermani, A. Zargar Kharazi, A promising antibacterial wound dressing made of electrospun poly (glycerol sebacate) (PGS)/gelatin with local delivery of ascorbic acid and pantothenic acid. J. Polym. Environ. **31**(6), 2504–2518 (2023)
32. M. Kharaziha et al., PGS: gelatin nanofibrous scaffolds with tunable mechanical and structural properties for engineering cardiac tissues. Biomaterials. **34**(27), 6355–6366 (2013)
33. F. Farhat, S.S. Sohail, F. Siddiqui, R.R. Irshad, D.Ø. Madsen, Curcumin in wound healing—a bibliometric analysis. Life. **13**(1), 143 (2023)
34. S. Alven, X. Nqoro, B.A. Aderibigbe, Polymer-based materials loaded with curcumin for wound healing applications. Polym. (Basel). **12**(10), 2286 (2020)
35. Y. Panahi et al., Antioxidant effects of curcuminoids in patients with type 2 diabetes mellitus: a randomized controlled trial. Inflammopharmacology. **25**, 25–31 (2017)
36. G.D. Venkatasubbu, T. Anusuya, Investigation on curcumin nanocomposite for wound dressing. Int. J. Biol. Macromol. **98**, 366–378 (2017)
37. Y. Zhao et al., A novel curcumin-loaded composite dressing facilitates wound healing due to its natural antioxidant effect. Drug Des. Devel Ther. **13**, 3269–3280 (2019)
38. N. Fereydouni et al., Curcumin nanofibers for the purpose of wound healing. J. Cell. Physiol. **234**(5), 5537–5554 (2019)
39. S.A. Ayati Najafabadi, P. Shirazaki, A. Zargar Kharazi, J. Varshosaz, M. Tahriri, L. Tayebi, Evaluation of sustained ciprofloxacin release of biodegradable electrospun gelatin/poly (glycerol

sebacate) mat membranes for wound dressing applications. Asia-Pacific J. Chem. Eng. **13**(6), e2255 (2018)
40. M. Suhaeri et al., Novel skin patch combining human fibroblast-derived matrix and ciprofloxacin for infected wound healing. Theranostics. **8**(18), 5025 (2018)
41. F. Zhou et al., Zinc ions and ciprofloxacin-encapsulated chitosan/poly (ε-caprolactone) composite nanofibers promote wound healing via enhanced antibacterial and immunomodulatory. Int. J. Biol. Macromol. **253**, 127086 (2023)
42. S.M.R. Hosseini et al., Carboxymethyl cellulose/sodium alginate hydrogel with anti-inflammatory capabilities for accelerated wound healing; in vitro and in vivo study. Eur. J. Pharmacol. **976**, 176671 (2024)
43. P. Heydari, J. Varshosaz, M. Kharaziha, S.H. Javanmard, Antibacterial and pH-sensitive methacrylate poly-L-Arginine/poly (β-amino ester) polymer for soft tissue engineering. J. Mater. Sci. Mater. Med. **34**(4), 16 (2023)
44. P. Heydari, M. Kharaziha, J. Varshosaz, A.Z. Kharazi, S.H. Javanmard, Co-release of nitric oxide and L-arginine from poly (β-amino ester)-based adhesive reprogram macrophages for accelerated wound healing and angiogenesis in vitro and in vivo. Biomater. Adv. **158**, 213762 (2024)
45. M. Buzgo et al., Poly-ε-caprolactone and polyvinyl alcohol electrospun wound dressings: adhesion properties and wound management of skin defects in rabbits. Regen Med. **14**(5), 423–445 (2019)
46. L. Moradkhannejhad, M. Abdouss, N. Nikfarjam, M.H. Shahriari, V. Heidary, The effect of molecular weight and content of PEG on in vitro drug release of electrospun curcumin loaded PLA/PEG nanofibers. J. Drug Deliv Sci. Technol. **56**, 101554 (2020)
47. C. Cui et al., Optimizing the chitosan-PCL based membranes with random/aligned fiber structure for controlled ciprofloxacin delivery and wound healing. Int. J. Biol. Macromol. **205**, 500–510 (2022)
48. A. Dodero, E. Brunengo, M. Alloisio, A. Sionkowska, S. Vicini, M. Castellano, Chitosan-based electrospun membranes: effects of solution viscosity, coagulant and crosslinker. Carbohydr. Polym. **235**, 115976 (2020)
49. T.A. Jeckson, Y.P. Neo, S.P. Sisinthy, J.B. Foo, H. Choudhury, B. Gorain, Formulation and characterisation of deferoxamine nanofiber as potential wound dressing for the treatment of diabetic foot ulcer. J. Drug Deliv Sci. Technol. **66**, 102751 (2021)
50. J. Xia, H. Zhang, F. Yu, Y. Pei, X. Luo, Superclear, porous cellulose membranes with chitosan-coated nanofibers for visualized cutaneous wound healing dressing. ACS Appl. Mater. Interfaces. **12**(21), 24370–24379 (2020)
51. U. Meyer, T. Meyer, J. Handschel, H.P. Wiesmann, *Fundamentals of Tissue Engineering and Regenerative Medicine* (Springer, 2009)
52. J. Amirian et al., In-situ crosslinked hydrogel based on amidated pectin/oxidized chitosan as potential wound dressing for skin repairing. Carbohydr. Polym. **251**, 117005 (2021)
53. J. Wu et al., Electrospun nanofiber scaffold for skin tissue engineering: a review. ACS Appl. Bio Mater. **6**, 3556–3567 (2024)
54. B. Beiki, B. Zeynali, E. Seyedjafari, Fabrication of a three dimensional spongy scaffold using human Wharton's jelly derived extracellular matrix for wound healing. Mater. Sci. Eng. C **78**, 627–638 (2017)
55. M. Sadeghi, M. Rahimnejad, H. Adeli, F. Feizi, Matrix–drug interactions for the development of pH-sensitive alginate-based nanofibers as an advanced wound dressing. J. Polym. Environ. **31**(3), 1242–1256 (2023)
56. Z. Jiang et al., Nanofiber scaffolds as drug delivery systems promoting wound healing. Pharmaceutics. **15**(7), 1829 (2023)
57. A. Guzmán-Soria, V. Moreno-Serna, D.A. Canales, C. García-Herrera, P.A. Zapata, P.A. Orihuela, Effect of electrospun PLGA/collagen scaffolds on cell adhesion, viability, and collagen release: potential applications in tissue engineering. Polym. (Basel). **15**(5), 1079 (2023)
58. M. Li et al., Hydrogel/nanofibrous membrane composites with enhanced water retention, stretchability and self-healing capability for wound healing. Compos. Part. B Eng. **257**, 110672 (2023)
59. S. Nauman, G. Lubineau, H.F. Alharbi, Post processing strategies for the enhancement of mechanical properties of enms (Electrospun Nanofibrous membranes): a review. Membr. (Basel). **11**(1), 39 (2021)
60. T.U. Rashid, R.E. Gorga, W.E. Krause, Mechanical properties of electrospun fibers—a critical review. Adv. Eng. Mater. **23**(9), 2100153 (2021)
61. H.H. Kim, M.J. Kim, S.J. Ryu, C.S. Ki, Y.H. Park, Effect of fiber diameter on surface morphology, mechanical property, and cell behavior of electrospun poly (ε-caprolactone) mat. Fibers Polym. **17**, 1033–1042 (2016)
62. M. Abasalta, A. Asefnejad, M.T. Khorasani, A.R. Saadatabadi, Fabrication of carboxymethyl chitosan/poly (ε-caprolactone)/doxorubicin/nickel ferrite core-shell fibers for controlled release of doxorubicin against breast cancer. Carbohydr. Polym. **257**, 117631 (2021)
63. M.F. Abdullah, T. Nuge, A. Andriyana, B.C. Ang, F. Muhamad, Core–shell fibers: design, roles, and controllable release strategies in tissue engineering and drug delivery. Polymers (Basel) **11**(12), 2008 (2019)
64. K. Sangeetha, M.F. Albeshr, K. Shoba, G. Lavanya, P.S. Prasad, P.N. Sudha, Evaluation of cytocompatibility and cell proliferation of electrospun chitosan/polyvinyl alcohol/montmorillonite clay scaffold with l929 cell lines in skin regeneration activity and in silico molecular docking studies. Int. J. Biol. Macromol. **268**, 131762 (2024)
65. C. Vater et al., Effects of lecithin-based nanoemulsions on skin: short-time cytotoxicity MTT and BrdU studies, skin penetration of surfactants and additives and the delivery of curcumin. Int. J. Pharm. **580**, 119209 (2020)